ShrinkCells: Localized and Sequential Shape-Changing Actuation of 3D-Printed Objects via Selective Heating

Kongpyung (Justin) Moon
Industrial Design KAIST
jkpmoon@kaist.ac.kr

Haeun Lee
Industrial Design KAIST
chromium0624@kaist.ac.kr

Jeeeun Kim
Computer Science & Engineering Texas A&M University
jeeeun.kim@tamu.edu

Andrea Bianchi
Industrial Design KAIST
andrea@kaist.ac.kr

ABSTRACT

The unique behaviors of thermoplastic polymers enable shape-changing interfaces made of 3D printed objects that do not require complex electronics integration. While existing techniques rely on external trigger, such as heat, applied globally on a 3D printed object initiating all at once the shape-changing response (e.g., hot water, heat gun, oven), independent control of multiple parts of the object becomes nearly impossible. We introduce *ShrinkCells*, a set of shape-changing actuators that enables localized heat to shrink or bend, through combining the properties of two materials — conductive PLA is used to generate localized heat which selectively triggers the shrinking of a Shape Memory Polymer. The unique benefit of *ShrinkCells* is their capability of triggering simultaneous or sequential shape transformations for different geometries using a single power supply. This results in 3D printed rigid structures that actuate in sequence, avoiding self-collisions when unfolding. We contribute to the body of literature on 4D fabrication by a systematic investigation of selective heating with two different materials, the design and evaluation of the *ShrinkCells* shape-changing primitives, and applications demonstrating the usage of these actuators.

CCS CONCEPTS

• **Human-centered computing** → **Human computer interaction (HCI)**.

KEYWORDS

4D printing; Shape-changing; Selective Heating; Sequential actuation, Multi-material printing

1 INTRODUCTION

4D printing is a promising way to fabricate shape-changing objects that can self-actuate without motors or actuators integration [15]. Recent advances in materials made it possible for on-the-market thermoplastic polymers, such as PolyLactic Acid (PLA) and Thermoplastic Polyurethanes (TPU) which are commonly employed for low-cost 4D printing, to exert programmed buckling behaviors via their residual stress [7]; a heated polymer is stretched when 3D printed, which can be relieved by re-heating it above glass transition temperature (T_g, over 70° C for PLA [1]). Many inspired HCI researchers have proposed novel methods to take advantage of this property of heated thermoplastic for actuation, controlling it by adjusting the speed of the 3D printer's nozzle [1], infill densities [23], the layer thickness [31], or by combining mechanically dissimilar materials [1, 20], such thermoplastic polymers on a paper substrate [17, 29].

Existing 3D printed rigid artifacts designed to trigger a programmed shape-changing effect all at once are often heated via external stimuli that are applied on the whole 3D printed surface, such as a heat gun, hot water, or an in the oven [1, 30–32]. However, global heating is nearly impossible to selectively control certain portions of the object (perhaps close to each other) to heat and therefore to actuate, to what extent, or in which order. In contrast, other works [17, 20, 29] enable selective shape-changing of parts in an object via localized resistive heating (using conductive materials). Yet, the printed artifacts require manual intervention or an additional fabrication process to operate (e.g., heat-treatment or manual assembly).

To this end, we propose *ShrinkCells* , a set of novel 3D printed and rigid localized shape-changing actuators that can be sequentially triggered via selective heating after 3D printing, requiring no ad-hoc treaments for post-processing. Specifically, by combining the resistive heating properties of conductive filaments [29] with the shape-changing characteristics of 3D printable Shape-Memory Polymer (SMP), we designed 3D printed mechanisms capable of shrinking and bending, and a fuse mechanism that enables sequential activation of modular cells without the need for additional electronics for control. The key benefit of *ShrinkCells* is that they enable *localized and timed* shape transformation of multiple parts of an object or within the object itself (e.g., unreachable by the user) while conserving the properties of rigid 3D structures and avoiding self-collisions.

To summarize, we contribute:

- A systematic exploration of the heat-triggered shrinking effect of Shape Memory Polymers, and strategies for selectively heating conductive PLA.
- The design of *ShrinkCells* , capable of actuation in different directions through selective heating, through a holistic exploration of shape-changing primitives.
- The design and evaluation of a fuse mechanism that can be combined with *ShrinkCells* to generate sequential actuation using a single power source.
- A fabrication pipeline that allows users to embed *ShrinkCells* in custom 3D objects, and validation through a set of applications.

2 RELATED WORK

Our work closely intersects prior works in 4D printed shape-changing interfaces through various material driven approaches and fabrication techniques. These includes self-morphing interfaces that respond to the environmental factors such as humidity [4, 24, 27, 34], or pH of solutions [12, 28]. Some of these works [e.g. 27] achieve a remarkable expansion of volume by 150% from the original, resulting in flat surfaces that bend which however, requires use of a special hydrophilic UV-curable polymer. Other shape-changing techniques leverage air pressure [18, 33] or magnetic fields Zhu et al. [35] that react with 3D printing magnetic responsive structures.

As our work benefits from utilizing low-cost, off-the-shelf filaments that can be 3D printed with Fused Deposition Modeling (FDM) machines, we closely study prior works to actuate such materials using **heat** as a trigger for shape-changing behavior. The next two subsections focus on heat-activated shape-changing 4D printing.

2.1 Globally heated thermoplastic materials

Thermoplastic material behaviors have been extensively used in many HCI research and digital fabrication domains because of their shape-memory characteristics and malleability. Several works have leveraged these properties to allow users to adapt or customize 3D printed artifacts via manual deformations [9, 11, 13, 22]. However, these works do not focus on the self-actuation of material (4D), so they are not further discussed in this paper.

Another line of research focuses on self-folding 3D objects by leveraging the built-in residual stress during the FDM printing process. During 3D printing, the heated molecular chain of a polymer is sheared and elongated across the printed direction, to be then fixed via rapid cooling with the extruder fan [7]. This results in residual stress built into the printed object that can be released when the polymer is re-heated above its glass transition temperature (*Tg*), causing bending along the printed direction [7].

Several prior works leveraged this behavior to achieve shape-changing actuation using a single [31] or multiple materials [1], large-scale surfaces [32], or time-dependent morphing [10] via manual placement of a pre-stretched elastic membrane between 3D printed objects. *ShrinCage* [23], a closely related work, used residual stress through infill density and metamaterial structure to construct geometries that fasten around objects, allowing to adjust them with perfectly fitting props.

However, these works use sources of heat that are globally applied to the overall printed object, like hot water or hot air from a heat gun. These, in some cases, limit the applicability of the printed objects (e.g. objects immersed in water cannot use electronics) preventing a wide adoption of the discovery, and do not allow for accurately selecting the parts of the objects to actuate.

2.2 Locally heated self-actuated shape-changing interfaces

By locally heating part of an object, it becomes possible to achieve a selective shape-changing memory effect for only the heated region in the object. This principle was well exemplified by *Foldio* [17] and *Printed Paper actuators* [29], two techniques that print conductive ink or filament on the top of a paper substrate or of a polymer tape (3M VHB tape). When current flows through the conductive material, it generates heat thanks to the material's resistance (resistive heating) [5]. When the heat rises to the glass transition temperature, the conductive material [29] or the special polymer tape attached to it [17], contracts, causing the paper to bend. The limitation of this work is that only the conductive filament to furnish heating is 3D printed, while the target object is made of paper which could be too weak to afford real-world applications and is manually fabricated or assembled. The opposite approach is used by *Exoform*[20], which allows a user to 3D print custom PLA objects, but the source of heating and shape-changing — a multi-layer structure made of copper tape, a 3M VHB tape, and carbon nanotubes and polyborosiloxane — is manually applied on the top of the object.

Similar to these works [1, 20, 29], this paper presents a method for localized resistive heating that can generate selective shape-changing actuation. However, we uniquely create and evaluate rigid plastic actuators (*ShrinkCells*) that are completely 3D printed thus do not require manual assembly.
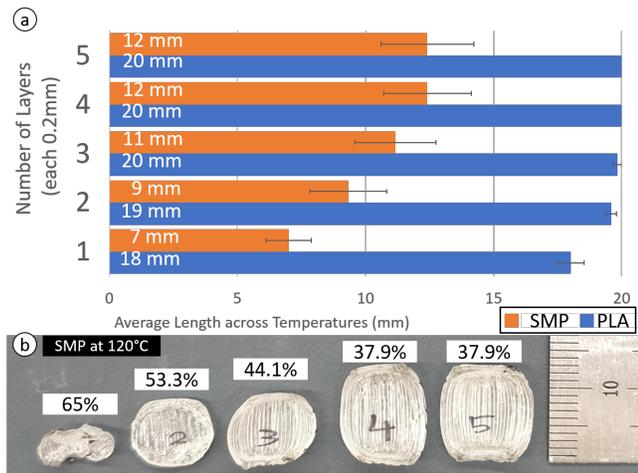
3 UNDERSTANDING SELECTIVE HEATING OF SMP AND CONDUCTIVE MATERIAL

The proposed shape-changing mechanism of *ShrinkCells* described in this paper is constructed using two off-the-shelf polymer filament materials for FDM 3D printing: a *Shape Memory Polymer (SMP)* filament, used for shrinking, and a carbon-composite conductive filament used for triggering the motion of SMP via local resistive heating. In this section, we systematically study the heating and shape-changing properties of these two materials.

3.1 SMP shrinking effect for different temperature and material thickness

SMP filament (*Kyoraku Co.*) is a thermoreactive *TPU* material that presents shape memory behavior when it reaches the glass transition temperature (Tg) of 60 °C [26]. At this temperature the filament becomes malleable, and if stretched through the printing process, its strong residual stress causes the material to shrink when heated.

Through a technical evaluation of material characteristics, we first aim to understand how changes in temperatures (applied globally) affect the shrinkage of 3D geometries printed using SMP and varying thicknesses (number of layers when the layer thickness is fixed). We compare these results to the effects of temperature on

Figure 1: (a) Average length of SMP and PLA samples with different number of layers after being heated, and (b) average shrink rate with representative five heated geometries

PLA (manufactured by FlashForge), another thermoplastic material which displays similar characteristics. We, therefore, created samples in five thicknesses, 1 to 5 layers, each 0.2 mm, covering the range 0.2 mm to 1.0 mm, and heated at six temperatures, from 70 °C to 120 °C with 10 °C interval.

30 samples for each SMP and PLA material were created following the specifications in previous work to obtain residual stress [1]. The printed samples have a dimension of 10 mm × 20 mm and are constructed from 25 longitudinal paths along the shrinking direction and 2 lateral paths (at the top and bottom of the structure) spanning the entire width of 10 mm. All the samples were printed using a direct drive extruder (FlashForge Creator 3, with 0.4 mm nozzle diameter) at 200 °C, with a speed of 5000 mm/min, and following the same paths. While the lateral paths affect the longitudinal shrinkage, their impact is minimal (at most 4%); therefore lateral paths are not considered as study parameters to find the shrinkage behaviors of SMP and PLA across temperatures.

Samples were then placed all at once in an oven (Puhui T-962 Infrared IC heater) for 1 minute and then, after cooling, we measured their length (L) with a Vernier caliper to compute a shrink ratio: $1 - L_{heated}/L_{original}$. In total, we heated 60 samples — 6 temperatures × 5 thickness × 2 materials.

The average length after shrinking across the six temperature settings is reported per layer in Figure 1. SMP material shows overall a greater shrinking effect than PLA (48% vs 3%), with a maximum shrunk length of 13 mm (SD: 2.17, 65% from the original length) for the 1-layer thick sample, compared to 2 mm (SD: 1.3, 10% shrink-rate) of PLA.

The number of printed layers also affected the shrink rate, by damping the heat transition. Thus, for SMP, the sample with a single layer (1 layer, 0.2 mm) shrunk 71% more than the thickest (5 layers) sample. However, we also note that the thinnest layer is deformed with warping imperfections probably due to the excessive heat than it can endure.

3.2 Understanding Joule-heating in 3D printed conductive filament

This section describes the evaluation of the interplay between 3D printed geometry using conductive PLA and the heat produced by an electric current passing through a conductive element (an effect known as Joule-heating or resistive-heating [5]). Understanding this process is critical, in that, while previous work explores the relationship between *resistance* and the cross-sectional area of printed conductive filament[8], the characterization of how temperature depends on printed geometry and supplied current (e.g., number of layers, maximum current ratings) has not been studied.

Thus, we aim to assess three key parameters of Joule-heating a conductive filament; 1) the **maximum current** value for heating the conductive material without damaging the 3D printed geometry; 2) how temperature changes as a function of the **cross-sectional area**; and 3) **heat distribution** in single 3D printed body with varying cross-sectional areas.

3.2.1 Materials, Dimensions, and method. For the following experiments, we used the *Protopasta* [19] electrically conductive composite PLA filament, chosen for its ready availability and rated with a volume resistivity of molded resin (not 3D printed) of 15 Ω/cm.

We 3D printed five conductive cuboid samples with 100% infill, fixed length, and height (50 mm × 1 mm, as in [8]), but varying cross-sectional areas, by linearly incrementing their width (0.8 mm to 2.4 mm with 0.4 mm intervals — same as nozzle size). This process resulted in the following cross-section areas and resistances: $0.8mm^2$ (25 $K\Omega$), $1.2mm^2$ (18.2 $K\Omega$), $1.6mm^2$ (14.3 $K\Omega$), $2mm^2$ (13.3 $K\Omega$) and $2.4mm^2$ (10 $K\Omega$). The relation between cross-sectional area and resistance is shown in prior work [8].
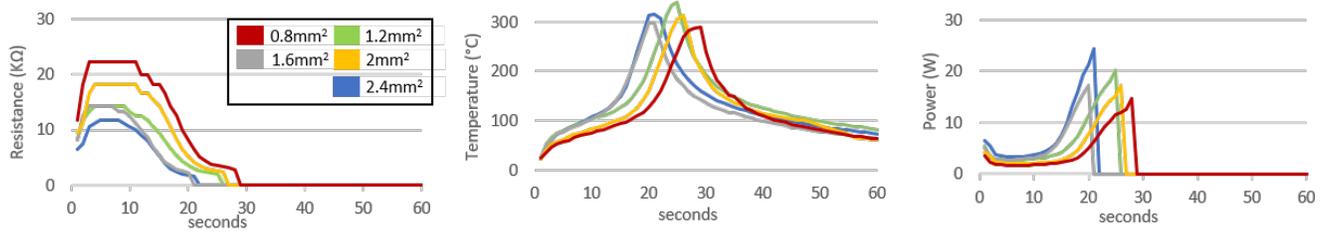
These cuboids were then attached to two copper wires at the extremities via two rectangular pads (4 mm × 4 mm) and connected to a DC power supply. Pads were coated using silver paste (*EL-COAT*, $1-3 \times 10^{-5}$ Ω/cm, 6 hours for drying) to minimize contact resistance with the powering wires and to better allow currents to flow through the cuboids. The conductive cuboids were printed on top of the PLA insulating substrate for better adhesion (Figure 2b).

Voltage and current from a DC power supply (Rohde and Schwarz NGA100) were remotely controlled via serial communication and a custom Python script running on a PC. The script samples at 1Hz voltage (V), current (I), and power (P), and automatically shuts down the power after the programmed duration. Temperatures were measured and recorded using a thermal video (infrared thermography) on a FLIR One Pro (emissivity 95%). The recording was then later analyzed via another Python script which used OpenCV [3] to extract the hottest temperature value on a legend for every second of the recorded video.

Laboratory safety precautions were used in conformity with institutional regulations: air filters, ventilation for fumes, overcurrent protection fuses, and no humans in the proximity of the voltage source when teleoperated.
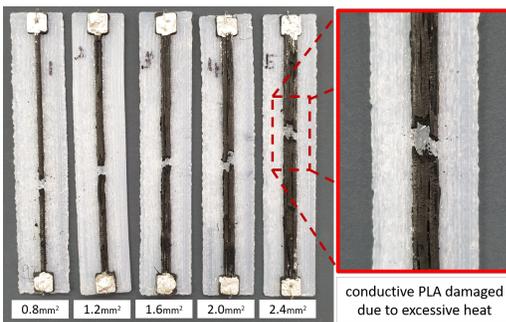
Experiment 1: Maximum current thresholds for continuous joule-heating of conductive filament

To better understand the design space, we first determined to identify the maximum current threshold for the printed material. We, therefore, powered the samples with the maximum ratings of our DC power supply (200 V at 400 mA) with constant voltage mode

Figure 2: Changes of resistance, temperature and power over time for five samples with varying cross-sectional areas. All samples melted within 30 seconds

and simultaneously recorded those values for 60 seconds. For all the samples, the recorded power values increased exponentially as the temperature rose. On average, power peaked at 18.7 W (SD:3.7), resulting in the temperature of 311 ℃ (SD: 20.4) and eventually melting the polymer around 23 seconds (SD: 3.9). Minimum and maximum values for each cross-section are shown in Figure 2.

Figure 3: All five samples were damaged by excessive heat

The experiment shows two findings. First, the cuboid with large cross-sectional areas heats up first (21 seconds vs. 28 seconds for the smallest cross-section cuboid). This is because a large cross section [8] corresponds to lower resistivity, allowing for a larger amount of current to pass through the conductor and generate heat.
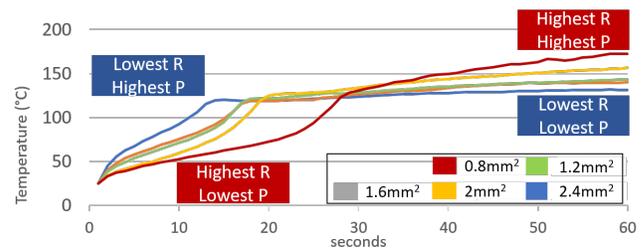
Second, the trend is exponential in the current load regardless of the cross-section area. This phenomenon occurs because the filament's resistance drops due to the polymer's structural relaxation beyond the glass temperature point ($Tg \geq 70℃$), forming stronger adhesion between the layers [21]. This stronger bondage between layers attains higher conductivity and consequently increases the current flow, further driving up the temperature.

For all samples, eventually, the average current peaked at 94 mA (19 W), generating an average peak temperature of 311 ℃ which caused the filament to melt and the power to shut. In conclusion, these combined results demonstrate that the larger cross-sections (lower resistance), the faster generated heat is, and that excessive current causes the material to melt regardless of cross-section areas.

Experiment 2: Heat comparison of varying cross-sectional areas with limited current

For the second assessment of material characters, we hypothesize that a wider cross-sectional area (lower resistance) will heat up

faster for a maximum current of 30 mA. This number was empirically derived from the data in Figure 2, which shows about 6.2 W in correspondence to the material's nominal melting point of 170℃. By setting this power threshold, we computed the current limit to 31 mA and approximated it to 30 mA. The experiment used the same materials and method described above.

Figure 4: Temperature with 30 mA maximum current

The results (Figure 4) show that with the maximum threshold current of 30 mA, no circuits melted. Furthermore, the wider cross-section cuboid indeed heated first (4 seconds vs 15 seconds of the thinnest), but it also had the lowest temperature (131℃). We note that, despite their different sizes, all samples powered with a current limit of 30 mA reached the glass transition temperature of 70℃. In fact, the hottest temperature was obtained by the thinnest of the cuboid (172℃ after 60 seconds) — the cuboid with the highest resistance.

This is because, if the current becomes constant after reaching the maximum threshold, power ($P=I^2R$) becomes a function only of resistance (if I^2 is a constant k, then $P=kR$). In other words, *after* the material reaches glass temperature and the current reaches its maximum, the temperature is further driven up by resistance alone, meaning that the *smaller* cross-section areas generate *more* heat.

Experiment 3: Heat distribution for varying cross-sections within a single geometry

In this final study, we aim to understand how heat is distributed over a single body with varying cross-sections along the length. From the previous experiment, we hypothesize that some portions in the structure with higher resistance (i.e., smaller cross-section areas) will also generate higher heat.

To systemically investigate all possible cases, we created cuboids of three cross-sections multiple of 0.8 mm^2 (the smallest cross-section in the previous study). This resulted in resistors of values:
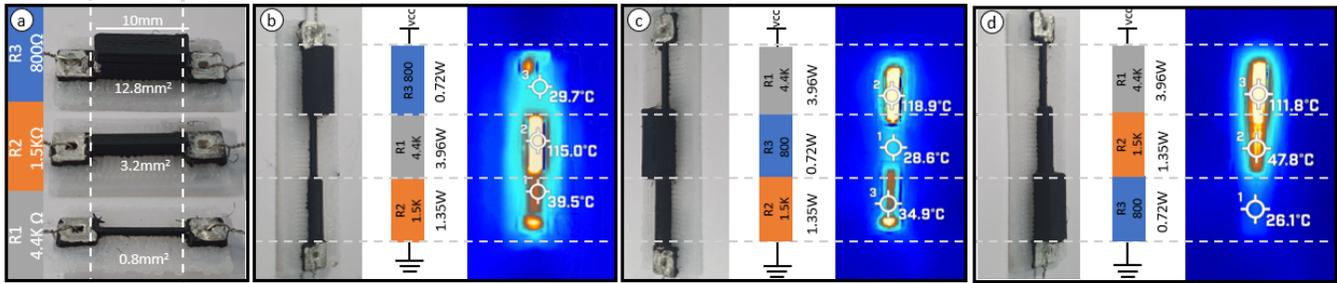
Figure 5: (a) Three resistors with varying cross-section, (b,c,d) the heat distribution for varying cross-section areas

$R1 = 0.8\ mm^2 = 4400\ \Omega$, $R2 = 3.2\ mm^2 = 1500\ \Omega$, and $R3 = 12.8\ mm^2 = 800\ \Omega$ (Figure 5-a), and printed them as a single solid structure in all the possible unordered permutations: R1-R2-R3, R1-R3-R2, and R3-R1-R2. The series-resistors amount to 7.4 KΩ (±5% accuracy), which includes the pads (350 Ω per pad). As before we applied a 200 V input voltage and 30 mA current limit.

The thermo-images in Figure 5-b,c,d illustrate that R1, the part of the geometry with the smallest cross-section (0.8 mm^2) and the highest resistance (4400 Ω) produces the largest amount of power (3.96 W) with an average temperature of 115.2 ℃, while R3, the parts of the geometry with the largest cross-section (12.8 mm^2) and the lowest resistance (800 Ω) generated only 0.72 W with an average temperature of 28.1 ℃ (below Tg).

These experiments confirm that, when 3D printed resistors with varying cross-section areas are connected in series, the power is internally distributed only as a function of the resistance of its parts (as demonstrated through the previous experiment) regardless of their order. This finding is clearly visible in Figure 5, and it shows the immediate applicability of being able to control which parts of the conductive filament should be heated, by purposely designing parts of the geometry with smaller cross-sectional areas.

3.3 Material study summary and guiding principles

In sum, we identify three key findings through the material exploration, that can be used for designing locally-heated activated shape-changing actuators:

- The ideal SMP substrate thickness to maximize shrinking without distortions is 2 layers (0.2 mm per layer)
- An appropriate current threshold for continuous Joule-heating with conductive filament must be set, depending on the heated geometry (30 mA for the cuboids in our experiments)
- In a structure with varying cross-section, the parts with lower cross-section (higher resistance) generates higher heat.

4 DESIGN AND EVALUATION OF SHRIKCELLS

We combine the properties of the SMP and conductive PLA filaments and the findings from the previous *Material section* to create shape-changing actuation primitives capable of shrinking and bending, called *ShrinkCells* . Specifically, with the aid of a dual nozzle

FDM printer (FlashForge Creator 3), we leverage both the shrinking properties of SMP material when heated above *Tg*, and the ability to selectively heat a portion of a 3D printed object by designing conductors with varying cross-sections. In this section, we detail the working principles for the operation of *ShrinkCells* , the implementation process, and the evaluation of actuated cells.

4.1 Principles of operation and design

A heated conductor sandwiched between two layers of SMP material can generate sufficient heat to trigger the shrinking of the SMP layers. Several prior works demonstrated the usage of heating elements (e.g., copper) placed within a 3D object [9, 20] or on the top of a paper substrate [17, 29] displaying buckling behaviors and shape-memory effect. However, the conductive material cannot shrink along with the surrounding material since structural shrinking [2] is not possible. Therefore, the naïve approach of simply layering SMP and conductive material produces an uncontrolled buckling behavior that tears the object apart (Figure 6).

Therefore, we designed a zigzag mechanism that is sandwiched by two SMP layers on each side. This mechanism provides continuous heat, and shrinks together with the surrounding SMP layers, without causing a buckling effect (Figure 6). By placing two conductive zigzag patterns on two separate layers isolated by a single SMP layer, we can also achieve *bending*, by allowing for shrinking only at one side of the geometry (i.e., shrinking either the top or bottom zigzag mechanism, or the left or right side of each mechanism).
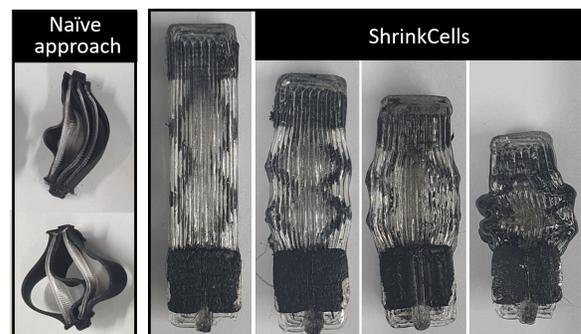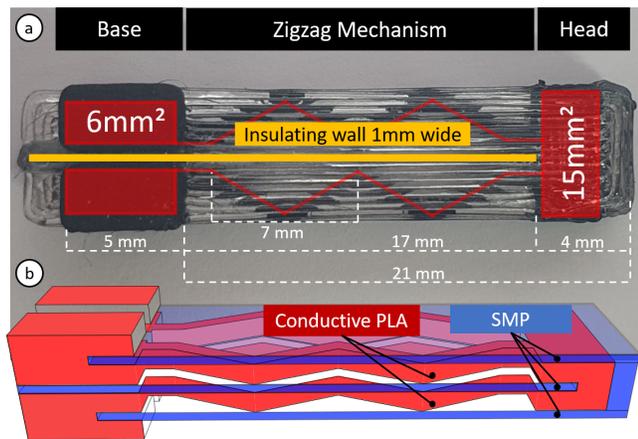

Figure 6: Buckling behavior of SMP layers when naïvely heated vs. *ShrinkCells*'s folding behavior

4.1.1 Implementation details. An actuation primitive (cell) is composed of a conductive *base* to be wired to the power, the shrinkage zone which is constructed using a pair of *zigzag mechanisms*, and a *head* that connects all the zigzag in a single node (Figure 7). All parts are printed in full material density to maximize their conductivity, with 100% infill setting for 3D printing.

Figure 7 illustrates the overall structure and its physical dimension. The *base* is made of four separate blocks (6 mm^2 cross-section) that are connected to a power source, either directly using alligator clips, or attached to other conductive cells. The zigzag mechanisms (14 mm length or longer) provide uniform heat while supporting the shrinking of the surrounding SMP layers (0.4 mm thick). When the SMP layer shrinks, the two arms of the zigzag mechanism start to fold in the shrinking direction. Each arm has a cross-section of 0.8 mm (1 mm layer thickness × 0.8 mm width).

Two of these mechanisms are placed on two separate layers insulated by a single SMP layer, while the arms are also insulated from each other with a 1 mm thick wall made of SMP. The zigzag mechanisms are connected with the *head*, which enables a return path for current back to the base. The different layers' thicknesses and the cross-sections rate were determined by the results in the *Material section.* Specifically, we intentionally designed the cross-section area of the zigzag mechanism to be smaller than the it of the head and the base. Because of the resulting higher resistance, heat is concentrated around the zigzag mechanism.
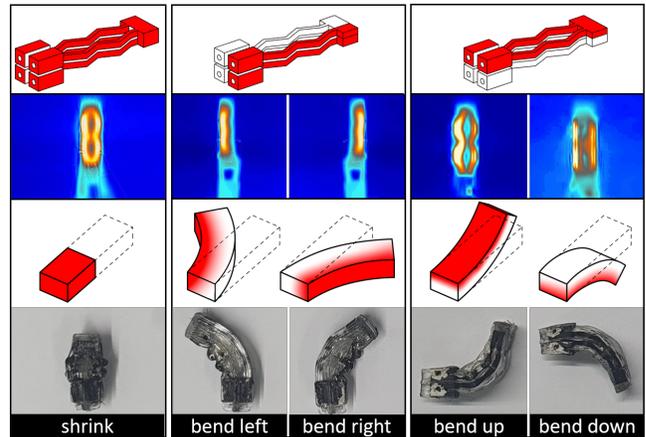

Figure 7: (a) Construction details of a *ShrinkCell*, and (b) layering PLA and SMP material

4.1.2 Type of motion actuation. By selectively heating different arms of the zigzag mechanisms, we can achieve three types of actuation: 1) shrinking, 2) bending, and 3) straightening after bending.

Shrinking: by powering both the zigzag mechanisms simultaneously, heat is generated uniformly (Figure 8) in the 3D geometry. This causes the SMP layers to heat up over *Tg* and shrink linearly. To achieve this, two base blocks are connected to the voltage source (Vcc) and the other two to the ground (GND).

Bending: by selectively heating any of the two arms of the zigzag structures, heat is generated only on one of the four sides of the cell (top, bottom, left, or right) as visible in Figure 8. This

Figure 8: Five different actuation by selective heating of the zigzag mechanism

relaxes the residual stress only on one side, resulting in a localized shrink. Effectively, when the cell located on one side shrinks while the rest remains still, the final shape results in the bending of the cell in one of the four directions.

Straightening: if a cell is bent on one side, the residual stress of the SMP in the direction of bending is used up, but the stress on the opposite side remains. By re-heating both the zigzag mechanisms, we can heat up and activate all the residual stress remaining in the SMP printed parts, causing them to straighten up and shrink simultaneously.

4.2 Technical Evaluations of Shape-Changing Actuation Cells

To understand the actuation capabilities of *ShrinkCells* , we conducted three experiments to characterize the design space: 1) the **shrink rate** as a function of the zigzag mechanism's length and applied current, 2) the pulling **force** that the cells can hold, and 3) the **bending angle** as a function of the cells' length. For all three experiments, we used freshly printed cells of five lengths (see Figure 10), for a cumulative total of 90 3D-printed test samples. All measures were sampled three times and averaged.

Experiment 1: Shrink rate of *ShrinkCells*

The first evaluation is designed to understand the maximum shrink rate of each *ShrinkCells* observed in five linearly incremental lengths (14 mm to 42 mm, with 7 mm intervals) under three different current-threshold settings (20 mA, 30 mA, and 40 mA) for one minute. In total, we tested 45 samples (5 varying lengths × 3 varying current-thresholds × 3 samples).

Results (Figure 9) show that the shrink rate grows by both increasing the supplied current and the length of the cell, with the maximum value being 61% (SD: 8.27, minimum: 51% and maximum: 66%) in the 35 mm long cell which was powered by 40 mA of current (similar to the maximum shrink rate found from the prior study about SMP material behavior). However, interestingly, the longest cell (42 mm) resulted in the smallest shrink-rate (22%, SD: 1.48), possibly due to the high resistance (8.5 $K\Omega$).
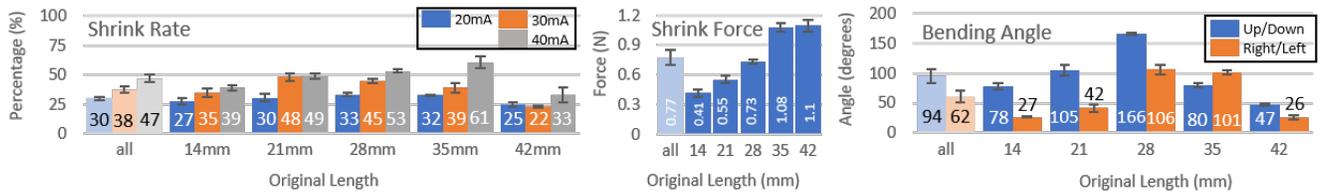
Figure 9: Results of average shrink rate, force, and bending angle for different currents and cell length
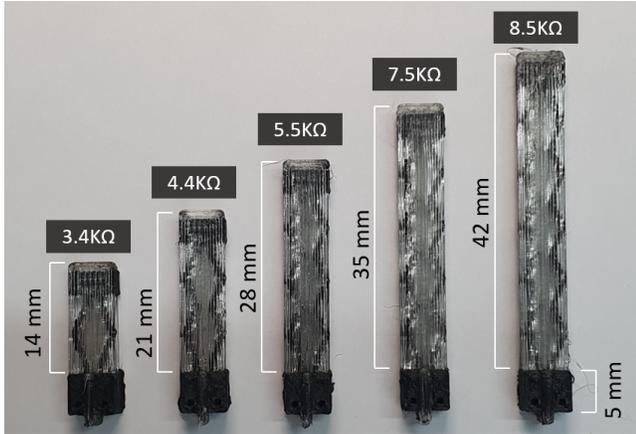

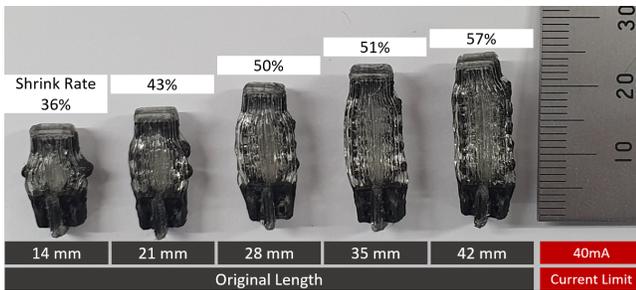Figure 10: Five samples of *ShrinkCells* used in the technical evaluations

Figure 11: Maximum shrink rates for varying length and 40 mA max current threshold
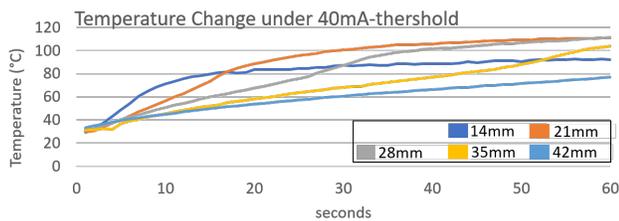

Figure 12: Temperature for varying length and 40 mA max current threshold

To better present this result, Figure 12 visualizes the temperature trend of five samples in different lengths when heated using 40 mA of maximum current. The graph illustrates how resistance (a function of length) affects the heating speed. For example, the 42 mm long cell (8.5 $K\Omega$) achieves glass transition temperature (70℃) within 48 seconds, while the slightly shorter 35 mm cell achieves it in 31 seconds. Shorter cells are faster to shrink (63 seconds faster), but they trade-off speed for a reduced shrink-rate (37% smaller shrink rate).

Experiment 2: Shrink force of *ShrinkCells*

The following experiment describes the shrink force produced by cells in five lengths, for a fixed current threshold of 40 mA. We measured the pulling force (N) for each cell by firmly holding it on a vise, while it pulls with an inflexible copper wire the tip of a gauge sensor (SHIMPO FGJN-5) placed onto it, following the same setup and method of previous work [25]. In total, we tested 15 cells (5 lengths × 3 repetitions).

Figure 9 shows the forces associated with each sample in various lengths. Force increases as the cell length increases (0.17 N average increase), but the longest cell only marginally increased the force of a +0.02 N from the second longest. The result implies that longer cells present a stronger pulling force, but this trend is limited when resistance grows beyond 7.5 $K\Omega$.
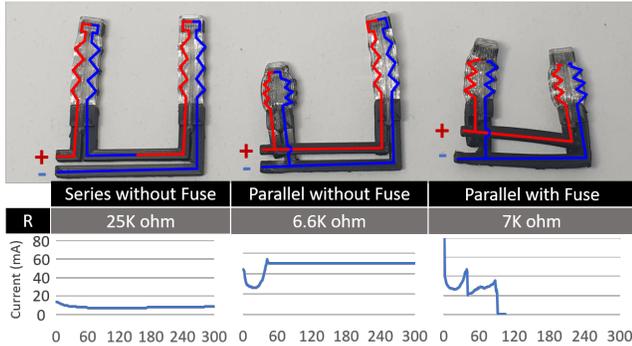
Experiment3: Bending angle of *ShrinkCells*

In this experiment, we aim to evaluate the maximum bending angle along with two representative bending directions (up and right) when the cell is heated to trigger the actuation (for 1 minute under the 40 mA current threshold). In total we tested 30 printed samples — 5 lengths × 2 bending directions × three times.

The first result (Figure 9) shows that the bending direction affects the maximum bending angle. Specifically, on average bending upward reached 94°(SD: 45) while sideways formed 61°(SD:40). This result is probably due to the differences in strength of the cell geometry in the two bending directions [14] — bending up or down has a lower tension because the layer thickness of the enclosing SMP layer is smaller (0.4 mm layer) than the width of the cell (6 mm). The second result shows that the greater bending angle is achieved with the 28 mm cell overall, regardless of the bending direction, suggesting a trade-off between length and actuation.

5 COUPLING OF *SHRINKCELLS*

This section focuses on strategies for bridging multiple *ShrinkCells* and achieving sequential activation. The obvious approach is to
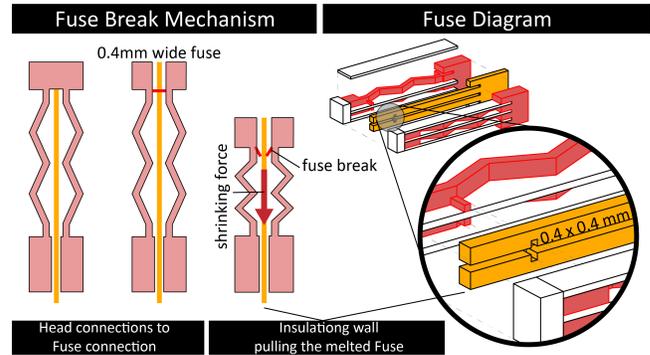
individually power each cell one by one at a time, or using separate power supplies as in previous work [6]. As these require user's manual interventions or additional controlling hardware (e.g., a micro-controller with sensors) which are certainly possible with *ShrinkCells* but not novel, and so not discussed in this section.
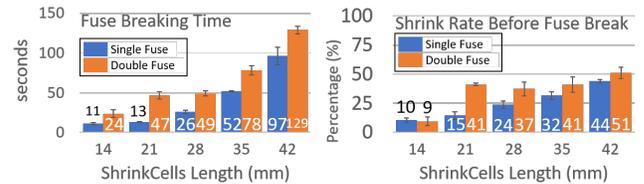

Figure 13: Naïve coupling of *ShrinkCells in-series* and *in-parallel* result in incorrect actuation vs. preventing over-heating with a fuse mechanism (right)

The most promising alternative considering the future design context is to use a single power supply with additional instrumentation for controlling multiple cells and to connect *ShrinkCells in series* or *in parallel*. In the following examples, we connected two *ShrinkCells* to a 200 V power supply with a 50 mA threshold current. *ShrinkCells* connected *in series* do not activate because the cumulative resistance of two cells is too large ($> 25\ k\Omega$). Thus, only a small current (8 mA) flows across the zigzag mechanisms, and heat cannot be generated (Figure 13). Connecting *ShrinkCells in parallel* activates the shrinking of both cells, but only if their resistive paths to the power source have identical resistance, causing the current to be equally divided between the two cells (e.g., 25 mA each). This requirement is difficult to verify as well as constraints where cells can be placed in a 3D printed object. When two *ShrinkCells* are connected *in parallel* instead and their resistance paths are different, both cells initially shrink together, but shortly after (in 50 seconds), the cell's higher resistance stops the shape-changing activation. This is because the cell with lower resistance heat and shrinks first, further decreasing its resistance, and taking an increasingly larger portion of the total current. This loop continues, resulting in one of the two cells being damaged, or, as in Figure 13, the full activation only of the cells with the initial lower resistance.

To solve these empirical challenges, we designed a 3D printed conductive electro-mechanical fuse that can interrupt the current flowing through a cell after a specific duration of time. By connecting cells with fuses in parallel, we achieve sequential and complete shape-changing activation (Figure 13). The cell with the smallest path resistance heats and shrinks first, eventually causing the fuse to blow. Once this occurs, the next cell receives full current flow and starts to activate subsequently.

Figure 14: The fuse mechanism (0.4×0.4 mm) connects two zigzag structures instead of the head (15 mm^2). The shrinking force of an insulating wall pulls down and breaks the fuse, stopping the current flow and the cell's shrinkage.
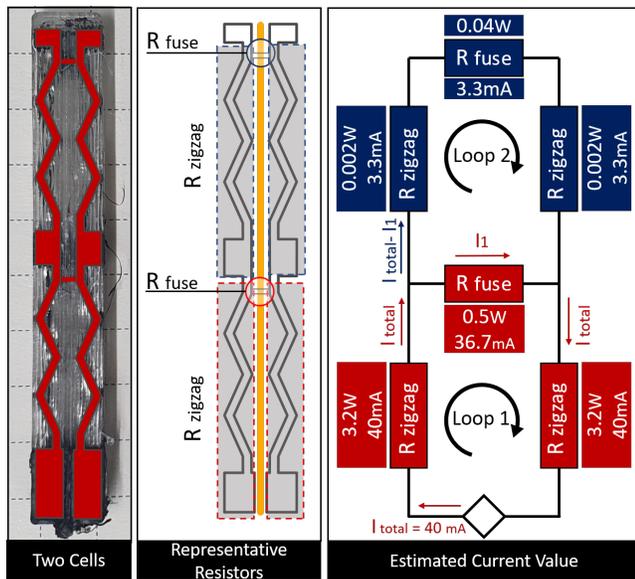

Figure 15: Average time for fuses to break, and shrink rate before fuses break

5.1 Actuation timing with a 3D printed fuse

The fuse is a small linkage (0.16 mm^2 cross-section) between the arms of a zigzag mechanism replacing the *head* thus permitting current to flow. The linkage has a smaller cross-section (higher resistance) than the zigzag mechanism so it heats up faster than the rest of the cell. The fuse is constructed like a small notch that interlocks with the central SMP wall separating the arms of the zigzag mechanism (Figure 14). When the fuse heats, this central wall also shrinks, tearing apart the fuse and breaking the connection between the zigzag arms. Use of two fuses (1 mm apart) can extend the duration of the actuation by creating a longer wait time. Although theoretically it is possible to design cells with more than two fuses, this may require a clever redesign of the zigzag mechanisms, because currently, it does not provide enough surface for attaching more than two fuses.

To identify the time needed for the fuses to trigger, we conducted additional experiments with cells shaped in different lengths, with one or two embedded fuses in the cells. We printed five *ShrinkCells* in identical dimensions to those in the three experiments described above (Figure 10) and powered them with 40 mA threshold. In total, we tested 5 lengths × 2 types of fuses × 3 times = 30 samples.

The fuses in all cells were successfully triggered, halting the current flow (Figure 15). The time taken to trigger the fuse increased by the length (resistance) of the cell, from 11 to 97 seconds for a single fuse and from 24 to 129 seconds for two fuses. On average, a single fuse took 39.6 seconds (SD: 5.4) to break, while two fuses took 65.3 seconds (SD 7.8) — about 60% longer than a single fuse. The

Figure 16: Schematic diagram on two connected cells showing the current flow in two cells placed in parallel. The current values are estimated by measuring the resistance of the zigzag structure and fuses of the *ShrinkCells* after printing (R-zigzag = 2000 Ω , R-fuse = 400 Ω).
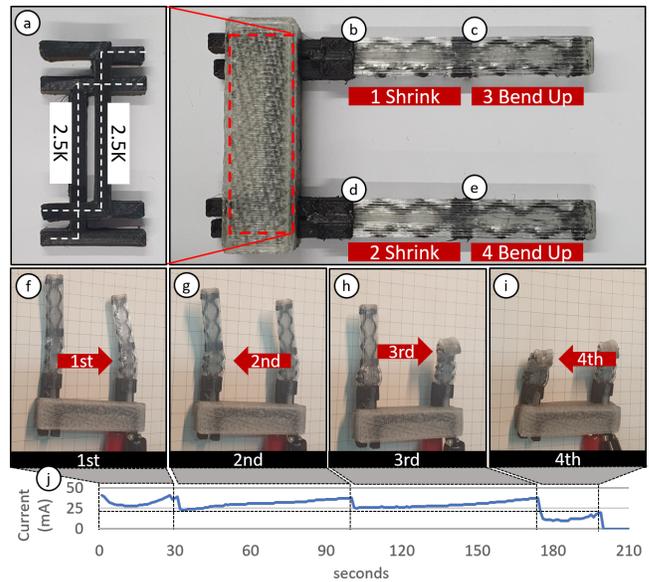
reason why the configuration with two fuses took more time is that two fuses form a parallel circuit, bisecting the current flowing in two paths. This results in less heat on each fuse, therefore, requires a longer time to stop the shrinkage compared to the structure with a single fuse.

Despite large variations in timing across samples of different lengths, the time at which the fuses broke was relatively predictable for specific lengths (the standard deviation shows a margin of error within 13%). In case of the timing is a significant design factor for some application design, Figure 15 also shows the shrink-rate achieved before the fuse is triggered – 24% (SD: 12) for a single fuse, and 36%(SD:16) for two fuses — the value similar to that reported for cells without fuses.

5.2 Sequential activation via fuses

Using fuses and conductive paths designed to designate specified resistances (as studied in [8]), we can achieve sequential activation of cells in predefined order — from the cell with the lowest resistance to the one with the largest resistance. As shown in Figure 17-a, we constructed a single *ShrinkCell* by using the head of the bottom cell as the base of the top cell. Each cell has its own fuse, which shorts the current and prevents it from heating the next cell. For example, the bottom cell in Figure 17-a heats up first because the majority of the current will flow through the path of least resistance (the bottom cell). Only after Fuse 1 blows, the current will go through the top cell.

This idea can be extended even further. Figure 17-right shows two double cells in parallel, and separated by the known resistance (5$k\Omega$). This setup results in a sequential activation: cell ⓑ is the

Figure 17: (a) Parallel connection with conductive material (b-e). Planned sequential activation of four cells, step-by-step actuation (f-i), and a graph showing when fuses blow (j)

closest to the power supply and the first one to activate. When its fuse blows, cell ⓓ activates, followed by cells ⓒ and then ⓔ. It is worth noting that all cells are independent: in this example, cells ⓑ and ⓓ shrink, while ⓒ and ⓔ bend.

This section demonstrates that it is possible to selectively and sequentially actuate *ShrinkCells* via the fuse timing mechanism. The order of activation depends on which path the current takes (the path of smallest resistance), while fuses are used to disconnect parallel sub-circuits. For a discussion on how to construct conductive paths of known resistances, the reader might refer to [8].

6 FABRICATION PIPELINE AND APPLICATIONS

To help users create various applications integrating *ShrinkCells* , we developed a design parametric script using the Grasshopper environment[1] for the Rhino 3D modelling tool. Our open-sourced software plugin[2] (Figure 18) automatically generates *ShrinkCells* from a simple cuboid geometry selected by a user, and based on specified design parameters: length of the zigzag mechanism (14 mm to 42 mm), number of fuses (single or dual-fuse), and the cell behavior (shrinking, bending), and the thickness of the conductive layer (i.e., size of the nozzle). While the tool allows users to tweak material dimensions further, it adapts the specific material parameters (e.g. cross-section of conductive materials and thickness of SMP) from the material study as a baseline. The tool exports a ready-to-print file in the STL format. Using this custom script, we designed and fabricated several example applications demonstrating the key benefits of *ShrinkCells* .

---

[1]https://www.rhino3d.com/features/#grasshopper
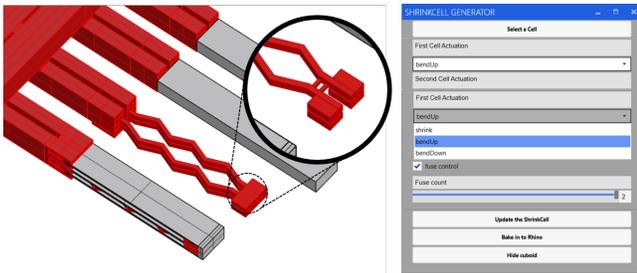[2]https://github.com/makinteractlab/ShrinkCells

Figure 18: *ShrinkCells* generator plugin for the Rhino 3D modelling environment

6.1 Applications

Many *ShrinkCells* can be combined together to compose **complex shape-changing transformations** (Figure 19). Four fingers of a 3D printed hand are replaced by *ShrinkCells* and activated in sequence to form a thumbs-up gesture, while the branches of a Christmas tree (three layers of five branches stacked to form a tree) are individually activated in four directions to convey an organic look to the 3D printed tree.
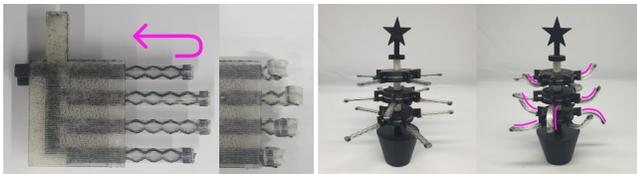

Figure 19: Self-folding fingers (left), and Christmas tree with branches in different directions (right)

A phone holder and a pen holder showcase the usage of timed **sequential actuation** of cells to avoid self collisions of un/folding geometries (Figure 20). The back stand part of a phone holder frame needs to unfold before the fixture of the leg on the opposite side bend to stabilize the phone.
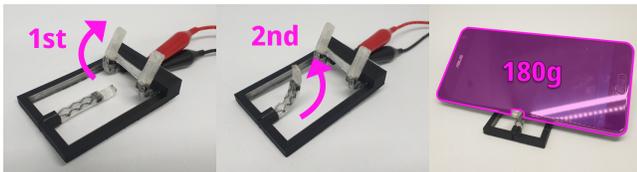

Figure 20: Sequentially unfolding a phone holder to prevent self-collisions

The folded hands of a pen holder shaped as a character also require sequential activation to avoid bumping into each other (Figure 21). When both hands rise, one at a time, they can uphold a pen, demonstrating that the final geometry remains rigid.

The **sturdiness** of the *ShrinkCells* cells when cooled and solidified after the programmed actuation is could be well exemplified by a self-folding mini table (60×40×2mm), which can easily withstand 500 ml of water (Figure 22).
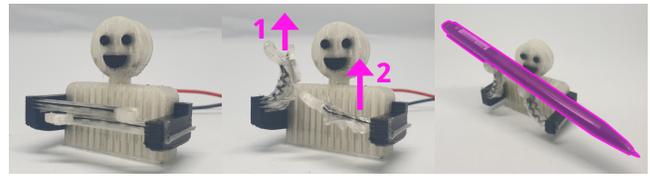

Figure 21: Sequentially unfolding the two arms to avoid self-collisions

Figure 22: Self-standing table that bears 500g after its shape-transformation

ShrinkCells also allows activation of cells placed *within* the object, instead of the *object's surface*. A locking mechanism built with a shrinking cell and enclosed inside of a rigid object can be activated even if a user cannot reach it directly(Figure 23-left). A 3D printed fastener can be inserted through a hole on the wall, fastened via bending two *ShrinkCells* in the opposite direction, and then re-heated for straightening again (Figure 23-right). Both applications demonstrate to which extent *ShrinkCells* can access indirectly and be controlled where users cannot reach.

Figure 23: A fastener actuates *inside a wall,* where it is not reachable (left). Actuating the inner (unreachable) mechanism of a lock (right)

Finally, a flower mood light and a 3D printed relay showcase the **integration of *ShrinkCells* with discrete external electronic components**. For the mood light, four discrete surface-mounted LEDs are integrated into the tips of the petals and connected in parallel with 3D printed fuses. When activated, these petals fold and the LEDs are slightly lit. Once the petals are completely folded, the fuses blow, and the LEDs become much brighter (Figure 24). A 3D printed relay demonstrates the integration of *ShrinkCells* with an external micro-controller board; when a cell shrinks it mechanically closes a switch allowing the current at the input of the relay to flow on the other side.

Figure 24: Discrete LEDs integrated in a shape-changing flower mood light (left), and a switch mechanism integrated with a micro-controller (right)

7 DISCUSSION, LIMITATIONS AND CONCLUSIONS

This paper extends prior work about activation of thermoplastic material behaviors that remember its initial shapes via heating [1, 31, 32], specifically leveraging localized resistive heating [17, 20, 29]. We contribute to the field of fabrication by extending prior knowledge about how multi-material substrate printed in SMP and conductive filaments behave when heated. We then introduced the *ShrinkCells*, a set of novel 3D printed rigid shape-changing primitives made of multi-material substrate using these two materials, and demonstrated how they achieve shrinking, bending, and straightening. Finally, we investigated how *ShrinkCells* can be coupled and used with a single power source, demonstrating sequential activation with examples of more complex shape transformations.

The main limitation of *ShrinkCells* is their applicability because the activation is not reversible — once shrunk, cells lose their residual stress, and no further actuation is possible. This makes *ShrinkCells* not ideal for applications that require continuous or repetitive actuation. We acknowledge this limitation but see the potential for usages that only require a one-time activation and permanent fixations (like [1, 11, 13]), but in part by part. Another limitation in its applicability is the high temperature demanded during the shape-transformation, which prevents users from designing applications that are associated with touching or wearing the *ShrinkCells* while being activated. Finally, because of the mechanical structure of the zigzag mechanism, *ShrinkCells* are only capable of shrinking in a congruent linear direction, limiting the motion primitives to bending and shrinking, which may constrain the type of application domain. Immediate future work could be incorporating twisting and coiling motions but would require a clever redesign of the folding mechanism.

The second main limitation is its scalability — the scale of the individual cells and how many cells can be connected with a single power source. This limitation depends upon the resistivity of the conductive element. We selected the *Protopasta* filament for its ready availability, but to decrease power ratings (e.g., lower than 200 V) while increasing the number of cells or the cells' size, better conductive carbon filaments such as copper-based 3D printable material (e.g., *Electrifi* [16]) or filament made of graphene might be considered in future studies to address this limitation. While these possible materials may require different current settings from ours (e.g., 40 mA threshold) for heating the SMP substrate, our material study procedure will serve future works as a baseline template to calibrate it and find the suitable current threshold. Furthermore,

combining *Protopasta* with lower resistive filaments such as *Electrifi* (0.006 Ω) might allow reducing the overall resistance of the connections by using *Protopasta* only as a heating element and not for electrical connections. This might result in more connected cells for the same total power provided to the 3D-printed artifact.

Finally, our software plugin and design pipeline are currently limited to the design of the cells from planar blocks, without accounting for non-planar input geometries nor for the length (i.e., resistance) of the conductive paths. The current plugin cannot simulate the current flow or inform the user of the ordering of activation of the *ShrinkCells*. The plugin is, in fact, agnostic to how long the users decide to heat the cells and only allows to define the type of actuation, not the duration of the exposure to heat. We could use fuses to interrupt the current flow at predictable yet fixed times, resulting in specific actuation. This is a possible extension for our future studies. Furthermore, the plugin does not allow to use of more than two fuses, nor to use of the cells' conductance for sensing input. Some of these limitations can probably be addressed in future work, and others will require manual interventions by the application designer.

Nonetheless, *ShrinkCells* opens the possibility to the integration of actuators embedded in 3D-printed objects that can be activated right after printing and without the need for external hardware (motors and micro-controllers), ultimately contributing to the vision of 4D printing.

ACKNOWLEDGMENTS

REFERENCES

[1] Byoungkwon An, Ye Tao, Jianzhe Gu, Tingyu Cheng, Xiang 'Anthony' Chen, Xiaoxiao Zhang, Wei Zhao, Youngwook Do, Shigeo Takahashi, Hsiang-Yun Wu, Teng Zhang, and Lining Yao. 2018. *Thermorph: Democratizing 4D Printing of Self-Folding Materials and Interfaces.* Association for Computing Machinery, New York, NY, USA, 1–12. https://doi.org/10.1145/3173574.3173834

[2] Shannon E. Bakarich, Robert Gorkin III, Marc in het Panhuis, and Geoffrey M. Spinks. 2015. 4D Printing with Mechanically Robust, Thermally Actuating Hydrogels. *Macromolecular Rapid Communications* 36, 12 (2015), 1211–1217. https://doi.org/10.1002/marc.201500079 arXiv:https://onlinelibrary.wiley.com/doi/pdf/10.1002/marc.201500079

[3] G. Bradski. 2000. The OpenCV Library. *Dr. Dobb's Journal of Software Tools* (2000).

[4] Tiffany Cheng, Yasaman Tahouni, Dylan Wood, Benjamin Stolz, Rolf Mülhaupt, and Achim Menges. 2020. Multifunctional Mesostructures: Design and Material Programming for 4D-Printing. In *Symposium on Computational Fabrication* (Virtual Event, USA) *(SCF '20)*. Association for Computing Machinery, New York, NY, USA, Article 11, 10 pages. https://doi.org/10.1145/3424630.3425418

[5] COMSOL. 2017. *The Joule Heating Effect.* https://www.comsol.com/multiphysics/the-joule-heating-effect

[6] Dongping Deng, Yang Yang, Yong Chen, Xing Lan, and Jesse Tice. 2017. Accurately controlled sequential self-folding structures by polystyrene film. *Smart Materials and Structures* 26, 8 (jul 2017), 085040. https://doi.org/10.1088/1361-665x/aa7a4e

[7] A. El Moumen, M. Tarfaoui, and K. Lafdi. [n.d.]. Modelling of the temperature and residual stress fields during 3D printing of polymer composites. 104, 5 ([n. d.]), 1661–1676. https://doi.org/10.1007/s00170-019-03965-y

[8] Patrick F. Flowers, Christopher Reyes, Shengrong Ye, Myung Jun Kim, and Benjamin J. Wiley. 2017. 3D printing electronic components and circuits with conductive thermoplastic filament. *Additive Manufacturing* 18 (2017), 156–163. https://doi.org/10.1016/j.addma.2017.10.002

[9] Daniel Groeger, Elena Chong Loo, and Jürgen Steimle. 2016. *HotFlex: Post-Print Customization of 3D Prints Using Embedded State Change*. Association for Computing Machinery, New York, NY, USA, 420–432. https://doi.org/10.1145/2858036.2858191

[10] Ruslan Guseinov, Connor McMahan, Jesús Pérez, Chiara Daraio, and Bernd Bickel. 2020. Programming temporal morphing of self-actuated shells. *Nature Communications* 11, 1 (13 Jan 2020), 237. https://doi.org/10.1038/s41467-019-14015-2

[11] Freddie Hong, Connor Myant, and David E Boyle. 2021. Thermoformed Circuit Boards: Fabrication of Highly Conductive Freeform 3D Printed Circuit Boards with Heat Bending. In *Proceedings of the 2021 CHI Conference on Human Factors in Computing Systems* (Yokohama, Japan) (*CHI '21*). Association for Computing Machinery, New York, NY, USA, Article 669, 10 pages. https://doi.org/10.1145/3411764.3445469

[12] Viirj Kan, Emma Vargo, Noa Machover, Hiroshi Ishii, Serena Pan, Weixuan Chen, and Yasuaki Kakehi. 2017. *Organic Primitives: Synthesis and Design of PH-Reactive Materials Using Molecular I/O for Sensing, Actuation, and Interaction*. Association for Computing Machinery, New York, NY, USA, 989–1000. https://doi.org/10.1145/3025453.3025952

[13] Donghyeon Ko, Jee Bin Yim, Yujin Lee, Jaehoon Pyun, and Woohun Lee. 2021. Designing Metamaterial Cells to Enrich Thermoforming 3D Printed Object for Post-Print Modification. In *Proceedings of the 2021 CHI Conference on Human Factors in Computing Systems* (Yokohama, Japan) (*CHI '21*). Association for Computing Machinery, New York, NY, USA, Article 671, 12 pages. https://doi.org/10.1145/3411764.3445229

[14] Qiushi Li, Wei Zhao, Yongxiang Li, Weiwei Yang, and Gong Wang. 2019. Flexural Properties and Fracture Behavior of CF/PEEK in Orthogonal Building Orientation by FDM: Microstructure and Mechanism. *Polymers* 11, 4 (2019). https://doi.org/10.3390/polym11040656

[15] Farhang Momeni, Seyed M.Mehdi Hassani.N, Xun Liu, and Jun Ni. 2017. A review of 4D printing. *Materials & Design* 122 (2017), 42–79. https://doi.org/10.1016/j.matdes.2017.02.068

[16] Multi3D. 2022. *Electrifi Conductive Filament*. https://www.multi3dllc.com/product/electrifi/

[17] Simon Olberding, Sergio Soto Ortega, Klaus Hildebrandt, and Jürgen Steimle. 2015. Foldio: Digital Fabrication of Interactive and Shape-Changing Objects With Foldable Printed Electronics. In *Proceedings of the 28th Annual ACM Symposium on User Interface Software & Technology* (Charlotte, NC, USA) (*UIST '15*). Association for Computing Machinery, New York, NY, USA, 223–232. https://doi.org/10.1145/2807442.2807494

[18] Jifei Ou, Mélina Skouras, Nikolaos Vlavianos, Felix Heibeck, Chin-Yi Cheng, Jannik Peters, and Hiroshi Ishii. 2016. AeroMorph - Heat-Sealing Inflatable Shape-Change Materials for Interaction Design. In *Proceedings of the 29th Annual Symposium on User Interface Software and Technology* (Tokyo, Japan) (*UIST '16*). Association for Computing Machinery, New York, NY, USA, 121–132. https://doi.org/10.1145/2984511.2984520

[19] Protopasta. 2022. *Protopasta Material Data*. https://www.proto-pasta.com/pages/high-temp-pla#HTmade

[20] Fang Qin, Huai-Yu Cheng, Rachel Sneeringer, Maria Vlachostergiou, Sampada Acharya, Haolin Liu, Carmel Majidi, Mohammad Islam, and Lining Yao. 2021. ExoForm: Shape Memory and Self-Fusing Semi-Rigid Wearables. In *Extended Abstracts of the 2021 CHI Conference on Human Factors in Computing Systems* (Yokohama, Japan) (*CHI EA '21*). Association for Computing Machinery, New York, NY, USA, Article 249, 8 pages. https://doi.org/10.1145/3411763.3451818

[21] K. Rodzeń, E. Harkin-Jones, M. Wegrzyn, P.K. Sharma, and A. Zhigunov. 2021. Improvement of the layer-layer adhesion in FFF 3D printed PEEK/carbon fibre composites. *Composites Part A: Applied Science and Manufacturing* 149 (2021), 106532. https://doi.org/10.1016/j.compositesa.2021.106532

[22] Andrew O. Sageman-Furnas, Nobuyuki Umetani, and Ryan Schmidt. 2015. Meltables: Fabrication of Complex 3D Curves by Melting. In *SIGGRAPH Asia 2015 Technical Briefs* (Kobe, Japan) (*SA '15*). Association for Computing Machinery,

New York, NY, USA, Article 14, 4 pages. https://doi.org/10.1145/2820903.2820915

[23] Lingyun Sun, Yue Yang, Yu Chen, Jiaji Li, Danli Luo, Haolin Liu, Lining Yao, Ye Tao, and Guanyun Wang. 2021. ShrinCage: 4D Printing Accessories That Self-Adapt. In *Proceedings of the 2021 CHI Conference on Human Factors in Computing Systems* (Yokohama, Japan) (*CHI '21*). Association for Computing Machinery, New York, NY, USA, Article 433, 12 pages. https://doi.org/10.1145/3411764.3445220

[24] Yasaman Tahouni, Tiffany Cheng, Dylan Wood, Renate Sachse, Rebecca Thierer, Manfred Bischoff, and Achim Menges. 2020. Self-Shaping Curved Folding: A 4D-Printing Method for Fabrication of Self-Folding Curved Crease Structures. In *Symposium on Computational Fabrication* (Virtual Event, USA) (*SCF '20*). Association for Computing Machinery, New York, NY, USA, Article 5, 11 pages. https://doi.org/10.1145/3424630.3425416

[25] Oliver Teall, Martins Pilegis, Robert Davies, John Sweeney, Tony Jefferson, Robert Lark, and Diane Gardner. 2018. A shape memory polymer concrete crack closure system activated by electrical current. *Smart Materials and Structures* 27, 7 (may 2018), 075016. https://doi.org/10.1088/1361-665x/aac28a

[26] SMP technologies. 2008. *Shape Memory Polymer Filament*. http://www.smptechno.com/index_en.html

[27] Skylar Tibbits. 2014. 4D Printing: Multi-Material Shape Change. *Architectural Design* 84, 1 (2014), 116–121. https://doi.org/10.1002/ad.1710 arXiv:https://onlinelibrary.wiley.com/doi/pdf/10.1002/ad.1710

[28] Elzelinde van Doleweerd, Ferran Altarriba Bertran, and Miguel Bruns. 2022. Incorporating Shape-Changing Food Materials Into Everyday Culinary Practices: Guidelines Informed by Participatory Sessions with Chefs Involving Edible PH-Responsive Origami Structures. In *Sixteenth International Conference on Tangible, Embedded, and Embodied Interaction* (Daejeon, Republic of Korea) (*TEI '22*). Association for Computing Machinery, New York, NY, USA, Article 9, 14 pages. https://doi.org/10.1145/3490149.3501315

[29] Guanyun Wang, Tingyu Cheng, Youngwook Do, Humphrey Yang, Ye Tao, Jianzhe Gu, Byoungkwon An, and Lining Yao. 2018. *Printed Paper Actuator: A Low-Cost Reversible Actuation and Sensing Method for Shape Changing Interfaces*. Association for Computing Machinery, New York, NY, USA, 1–12. https://doi.org/10.1145/3173574.3174143

[30] Guanyun Wang, Fang Qin, Haolin Liu, Ye Tao, Yang Zhang, Yongjie Jessica Zhang, and Lining Yao. 2020. MorphingCircuit: An Integrated Design, Simulation, and Fabrication Workflow for Self-Morphing Electronics. *Proc. ACM Interact. Mob. Wearable Ubiquitous Technol.* 4, 4, Article 157 (dec 2020), 26 pages. https://doi.org/10.1145/3432232

[31] Guanyun Wang, Ye Tao, Ozguc Bertug Capunaman, Humphrey Yang, and Lining Yao. 2019. A-Line: 4D Printing Morphing Linear Composite Structures. In *Proceedings of the 2019 CHI Conference on Human Factors in Computing Systems* (Glasgow, Scotland Uk) (*CHI '19*). Association for Computing Machinery, New York, NY, USA, 1–12. https://doi.org/10.1145/3290605.3300656

[32] Guanyun Wang, Humphrey Yang, Zeyu Yan, Nurcan Gecer Ulu, Ye Tao, Jianzhe Gu, Levent Burak Kara, and Lining Yao. 2018. 4DMesh: 4D Printing Morphing Non-Developable Mesh Surfaces. In *Proceedings of the 31st Annual ACM Symposium on User Interface Software and Technology* (Berlin, Germany) (*UIST '18*). Association for Computing Machinery, New York, NY, USA, 623–635. https://doi.org/10.1145/3242587.3242625

[33] Zeyu Yan and Huaishu Peng. 2021. *FabHydro: Printing Interactive Hydraulic Devices with an Affordable SLA 3D Printer*. Association for Computing Machinery, New York, NY, USA, 298–311. https://doi.org/10.1145/3472749.3474751

[34] Lining Yao, Jifei Ou, Chin-Yi Cheng, Helene Steiner, Wen Wang, Guanyun Wang, and Hiroshi Ishii. 2015. BioLogic: Natto Cells as Nanoactuators for Shape Changing Interfaces. In *Proceedings of the 33rd Annual ACM Conference on Human Factors in Computing Systems* (Seoul, Republic of Korea) (*CHI '15*). Association for Computing Machinery, New York, NY, USA, 1–10. https://doi.org/10.1145/2702123.2702611

[35] Pengfei Zhu, Weiyi Yang, Rong Wang, Shuang Gao, Bo Li, and Qi Li. 2018. 4D Printing of Complex Structures with a Fast Response Time to Magnetic Stimulus. *ACS Applied Materials & Interfaces* 10, 42 (2018), 36435–36442. https://doi.org/10.1021/acsami.8b12853 arXiv:https://doi.org/10.1021/acsami.8b12853